Chemical Engineering Journal 143 (2008) 314–325

Contents lists available at ScienceDirect

Chemical Engineering Journal

journal homepage: www.elsevier.com/locate/cej

Reduced discrete population balance model for precipitation of barium sulfate nanoparticles in non-ionic microemulsions

Björn Niemann[a], Kai Sundmacher[a,b,*]

[a] Max Planck Institute for Dynamics of Complex Technical Systems, Sandtorstraße 1, D-39106 Magdeburg, Germany
[b] Process Systems Engineering, Otto-von-Guericke University Magdeburg, Universitätsplatz 2, D-39106 Magdeburg, Germany

ARTICLE INFO

Article history:
Received 12 January 2008
Received in revised form 10 June 2008
Accepted 17 June 2008

Keywords:
Population balance
Nanoparticles
Nucleation
Growth
Microemulsion

ABSTRACT

A discrete population balance model is formulated in order to analyze the precipitation process of barium sulfate nanoparticles taking place in the droplets of a water-in-oil microemulsion. The model accounts for the distribution of reactants over the droplet population in terms of discrete numbers of the reacting ionic species (Ba^{2+}, SO_4^{2-}), as well as for the nucleation and growth of solid particles in terms of discrete $BaSO_4$-molecular units. The introduction of physically motivated assumptions leads to a considerable reduction of complexity of the population balance model. The kinetic parameters for nucleation and growth are estimated by fitting of simulated particle size distributions to recently published experimental data by Niemann et al. [B. Niemann, P. Veit, K. Sundmacher, Nanoparticle precipitation in reverse microemulsions: particle formation dynamics and tailoring of particle size distributions, Langmuir 24 (1), 2008, 4320–4328] and Adityawarman et al. [D. Adityawarman, A. Voigt, P. Veit, K. Sundmacher, Precipitation of $BaSO_4$ nanoparticles in a non-ionic microemulsion: identification of suitable control parameters, Chem. Eng. Sci. 60 (12), 2005, 3373–3381]. The obtained parameter values support the conclusion that particle nucleation follows a heterogeneous mechanism and that the nanostructure of the microemulsion has a significant effect on the particle growth mechanism. The considered microemulsion-assisted precipitation process allows the generation of nanoparticle morphologies which are not attainable by classical bulk phase precipitation processes.

1. Introduction

Nanoparticles are very often used as particulate precursors for advanced applications such as heterogeneous catalysts, semiconductors, ceramic materials, microelectronic devices, pharmaceutical ingredients and paint compounds. Especially particles with a size below 100 nm are of scientific and technological interest due to their unique physical and chemical properties. For example the melting point, the solubility, the surface hardness, the electrical conductivity and the surface reactivity of nano-scale materials can differ significantly from the properties of corresponding bulk materials [3]. Additionally, these properties do not only depend on the particle size but also on the shape of the particle size distribution (PSD). Therefore, it is an indispensable task for a tailored product design to apply a particle synthesis technique which allows the controlled adjustment of the mean particle size and the broadness of the PSD. Among different bottom-up methods like sol–gel processing, chemical vapor deposition, flame spraying synthesis and molecular condensation, precipitation inside the droplets of a water-in-oil-microemulsion (often referred to as "reverse micelles") is – on the laboratory scale – an established way for the controlled production of narrowly distributed nanoparticles [4,5].

A broad spectrum of different materials like metals [6], bimetals [7,8], metal oxides [9,10], borides [11], carbonates [12], halides [13], pharmaceuticals [14], semiconductors [15,16] and sulfates [17,18] has been successfully produced by precipitation in microemulsions. In general, two different modes for the initialization of the precipitation reaction can be distinguished. One can either transfer one reactant by mass transport from the continuous phase into the microemulsion droplets which already contain the other reactant (see e.g. [19]) or one can dissolve both reactants in two separate microemulsions, which are then macro-mixed by feeding one of the two microemulsions into a stirred tank reactor which is partly filled with the other microemulsion (see e.g. [20]). In the latter case, the reactants are finally micro-mixed by droplet exchange (i.e. by fusion and fission of the droplets). In both operating modes, the two reactants are contacted within the microemulsion droplets and

* Corresponding author at: Max Planck Institute for Dynamics of Complex Technical Systems, Sandtorstraße 1, D-39106 Magdeburg, Germany.
Tel.: +49 391 6110 350; fax: +49 391 6110 353.
E-mail address: sundmacher@mpi-magdeburg.mpg.de (K. Sundmacher).

1385-8947/$ – see front matter © 2008 Elsevier B.V. All rights reserved.
doi:10.1016/j.cej.2008.06.012

Nomenclature

a_i	parameter in Eq. (17), $i = 1–3$
c_A	concentration of component A [mol/l]
c_B	concentration of component B [mol/l]
c_{feed}	concentration of the feed component [mol/l]
$c_{reactor}$	concentration of the component inside the reactor [mol/l]
d_P	particle diameter [nm]
f	droplet number distribution
f_{ref}	reference droplet number distribution
G_i	individual growth rate for direction $i = x, y, z$ [nm/s]
k_B	Boltzmann constant [J/K]
$k_{gro,i}$	individual growth rate constant in $i = x, y, z$ direction [nm/s]
k_{gro}^{eff}	effective growth rate constant [nm/s]
k_L	solubility [mol^2/l^2]
k_{nuc}^{eff}	effective nucleation rate constant [$1/(m^3\,s)$]
M_P	molecular mass of the solid particle [g/mol]
N_A	number of A ions inside one droplet
N_A^t	total number of A ions inside the reactor
N_{A^*}	Avogadro's number [1/mol]
N_B	number of B ions inside one droplet
N_B^t	total number of B ions inside the reactor
N_{crit}	critical number of molecules needed to form a stable nucleus
N_{feed}	total number of droplets fed per second [1/s]
$N_{l,max}$	maximum number of dissolved reactant ions per droplet
N_M	total number of droplets in the reactor
$N_{M,0}$	initial total number of droplets in the reactor
N_P	number of $BaSO_4$ molecules (P) in one particle
N_P^t	total number of $BaSO_4$ molecules (P) in all particles inside the reactor
P_{2D}	two-dimensional probability density distribution
P_{2D}^{eq}	two-dimensional equilibrium probability density distribution
P_A	one-dimensional probability density distribution for dissolved A ions
P_B	one-dimensional probability density distribution for dissolved B ions
r_{gro}	growth rate [nm/s]
$r_{gro,0}$	reference growth rate without impurity consideration [nm/s]
r_{nuc}	nucleation rate [$1/(m^3\,s)$]
S	supersaturation
t	time [s]
t_{feed}	feeding time [s]
T	temperature [°C]
V_D	volume of one droplet [m^3]
V_P	particle volume [m^3]
$V_{W,0}$	initial volume of the water phase in the reactor [m^3]
x, y, z	space coordinates of the three-dimensional particle [nm]

Greek symbols

Δc_0	initial concentration difference [mol/l]
$\Delta d_{P,k}$	length of discretized particle size in element k [nm]
Θ	wetting angle for heterogeneous nucleation
α_{gro}	growth rate law exponent
α_{hex}	angle in the plate-like particles with a hexagonal main face
$\alpha_{imp}\cdot\theta$	surfactant adsorption correction function for growth
α_{nuc}	nucleation rate law exponent
ε	sum of error squares
λ_A	mean droplet occupancy with A ions
λ_A^{feed}	mean droplet occupancy in the feed with A ions
λ_B	mean droplet occupancy with B ions
ρ_P	particle density [g/cm^3]
σ	interfacial surface tension [J/m^2]
σ_{eff}	effective interfacial surface tension [J/m^2]
ζ_{redist}	redistribution control factor

consequently a chemical reaction starts which is followed by particle nucleation and growth. A scheme of this process is depicted in Fig. 1 along with a TEM picture of $BaSO_4$ nanoparticles which were synthesized using the two-emulsion method (see Niemann et al. [1]).

The excellent ability of microemulsion-assisted precipitation processes to synthesize nanoparticles with a well defined size and a narrow PSD is based on the distinguished physico-chemical properties of microemulsions. A microemulsion mixture consists of water, oil and a surfactant; sometimes two or more surfactants are used. If appropriate mass fractions of these components are mixed (for details see [21]), a thermodynamically stable emulsion can be generated. The size of the almost monodisperse microemulsion droplets is precisely adjustable in the range between 3 and 50 nm by the water-to-surfactant ratio and/or the temperature (for details see Rauscher et al. [22]). Within the water cores of these droplets, a limited amount of reactants can be dissolved. With regard to particle precipitation, it is of major importance that the use of a microemulsion as reaction medium leads to a slow-down effect for the precipitation process, and thereby to a better macro-mixedness of the reactor content at the time of onset of the precipitation in the droplets. This has been shown in the time-scale analysis by Rauscher et al. [22] and also in the computational fluid dynamics study by Öncül et al. [23]. Thus, almost identical particle formation conditions are guaranteed for the whole volume of the precipitation reactor. Furthermore, the precipitated nanoparticles are stabilized by the surfactant monolayer which surrounds each microemulsion droplet and thereby particle coagulation is suppressed. This effect was shown for a broad range of operating parameters [1]. Only the appearance of one reactant in large excess destabilizes the surfactant shells and then coagulation of particles can take place.

The model-based investigation of the particle formation mechanism is motivated by our previous experimental findings of barium sulfate precipitation in a non-ionic microemulsion (dispersed water droplets with a mean droplet diameter of 5 nm in a continuous cyclohexane oil-phase stabilized by the technical surfactant Marlipal O13/40 [1]). As important result of that work, a four-step mechanism for barium sulfate particle formation was formulated. The first step is the fusion–fission mechanism between the microemulsion droplets. The second step is the fast formation of nuclei initiated by the instantaneous chemical reaction

$$BaCl_2 + K_2SO_4 \rightarrow 2KCl + BaSO_4\downarrow . \quad (1)$$

The third step is the fast growth of particles in the droplets. Nucleation and growth are both significantly slowed-down by the droplet exchange phenomenon which decelerates the overall rate of particle formation. A particle growth barrier is identified when the particle size attains the size of microemulsion droplets. At a mean particle diameter (equivalent sphere diameter) of approximately 6 nm, particle growth is stopped in the majority of the

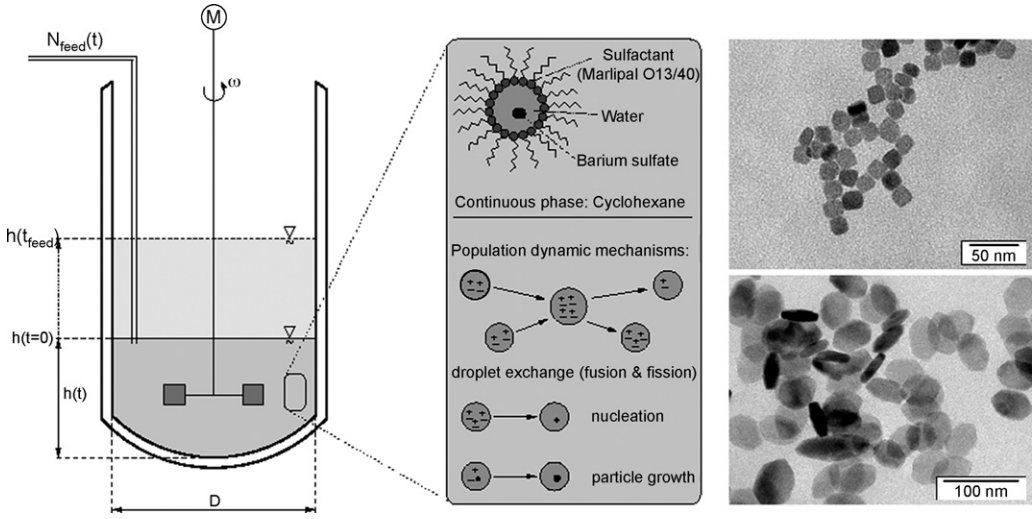

Fig. 1. Process scheme, population dynamic mechanisms and TEM picture of produced $BaSO_4$ nanoparticles.

experiments. This size of 6 nm corresponds to a swollen droplet size of approximately 7 nm, if a constant water volume during particle formation is assumed. Thus, the resulting water layer has a thickness of 0.5 nm and water-free domains are presumably lost completely (i.e. all water molecules are bound to the surfactant molecules or the particle surface). Such a state with very strongly bound molecules can reduce the film flexibility of the surfactant shell and therefore strongly decrease the droplet exchange rate and consequently decrease the particle growth rate. Crossing of the particle growth barrier is only possible by a fourth mechanistic step, i.e. the coagulation of the nanoparticles initiated by large excess of one reactant.

The just mentioned growth barrier can be quantified in terms of the initial concentration difference

$$\Delta c_0 = |c_{\text{reactor}} - c_{\text{feed}}|_{t=0}. \quad (2)$$

Above a Δc_0-value of approximately 0.075 mol/l, particles are able to cross the barrier and to form significantly larger particles, which change their morphology from an almost spherical particle to plate-like crystals with a dominant quadratic, rectangular or hexagonal face. Below this value all applied experimental conditions resulted in a similar PSD with a low polydispersity and a mean particle size of approximately 6 nm. Above this value mean particle sizes of 50 nm can be obtained. In general, the following micro-kinetic effects might be responsible for the observed growth behavior:

- Surfactant-directed growth, where the surfactant shells act as a template structure for the particle (see Mann and Ozin [24]),
- crystal face-specific adsorption effects of the surfactant molecules, which can lead to a growth-rate reduction of specific crystal faces (see Kubota and Mullin [25]),
- inherently different face-specific growth rates (see Zhang and Doherty [26]).

These mechanisms might also overlap, e.g. inherently different face-specific growth rates can be coupled with adsorption of surfactant molecules. The first effect, surfactant-directed growth, seems to be quite unlikely due to the fact that drastic structural changes of the microemulsion were necessary. The second and third effects fit much better to the experimentally observed growth behavior. Both have a similar impact on particle morphology, but a completely different micro-kinetic basis which has to be reflected by reasonable growth rate approaches in the model which is presented in Section 2.

Modeling and simulation of the considered microemulsion process is a challenging task, because at least three internal coordinates (distributed droplet properties) have to be considered for a complete representation of this complex system [23,27]. The three coordinates are the number of dissolved barium ions, N_A, the number of dissolved sulfate ions, N_B, and the number of barium sulfate molecules being in solid state, N_P, which quantifies the particle size. All three variables N_A, N_B and N_P are discrete. This fact has to be considered in the formulation of adequate rate expressions for nucleation and growth, as well as in the mass balances for the droplet population. By formulating the whole model in terms of the three discrete variables, any discretization error is avoided which is the major advantage of this approach. But the inclusion of all three coordinates can only be implemented adequately if the following additional assumptions will be made:

(a) The reactor is ideally macro-mixed (proved by CFD studies [23]),
(b) all droplets have the same water content,
(c) each droplet does not contain more than one particle.

Assumption (b) is formulated in this form, because microemulsion droplets are found to be nearly monodisperse if they contain no particles. If they contain a particle assumption (b) does not neglect the swelling of the droplet due to the growing particle, although the amount of swelling droplets will be very small (<0.5%). Assumption (c) reflects the fact that the probability for the appearance of more than one particle per droplet is negligibly small due to the low occupancy of the droplets with particles.

Comparable theoretical works in the field of nanoparticle synthesis in microemulsion droplets differ much from the here formulated model with regard to the considered population dynamic mechanisms, the number of distributed droplet properties and the used numerical solution technique. With respect to the last aspect, these models (see overview in [28]) can be classified into two groups, namely stochastic models [29–37] which comprehend stochastic population balance equations, Monte-Carlo simulation models, and deterministic models [10,15,19,38–40] where the latter comprise population balance models, moment models and simple analytical solutions. The main difference between models of the two groups lies in the complexity which is taken into account to achieve a solution at reasonable computational effort. Stochastic

models have the advantage that the computational effort is almost independent of the number of internal coordinates and therefore very complex systems can be implemented. However, the high number of necessary repeated simulation runs to attain statistical independence results in long simulation times in the order of days and a high demand of computer memory [41]. Consequently, such models are usually inappropriate for extensive parameter estimations, online process control or computational fluid dynamic (CFD) studies, which are important aspects for a later technical realization of such a process. These tasks can be analyzed by means of deterministic models which have to be less detailed concerning the number of internal coordinates. This requirement originates mainly from the droplet exchange mechanism represented by a multidimensional aggregation-type integral term. With the currently available computer power at maximum two coordinates can be handled in an efficient way, thus limiting the complexity of deterministic models. Deterministic models found in literature are in general strongly simplified to avoid multidimensional integral terms and therefore, in the majority of these models, only the mean particle size, mean concentrations or moments of the distributed properties are considered. The main disadvantage of such simplifications is the loss of important information like the shape of the PSD, which is an important indicator for product quality.

The deterministic model presented in this work is a compromise between the two above mentioned model groups. On the one hand a careful model reduction guarantees the applicability of parameter estimation procedures and on the other hand a relatively high complexity is obtained by a sophisticated implementation of all three distributed properties with the help of discrete stochastic functions. The model reduction is mainly focused on an alternative description of the droplet exchange term by the application of an equilibrium hypothesis and the transfer of the slow-down effect from the droplet exchange to the kinetic parameters of nucleation and growth rates. This reduction procedure enables the consideration of all internal coordinates in a deterministic model together with a realistic description of the stochastic redistribution of the ions during the droplet exchange. The distributed character of dissolved ions is taken into account in the particle formation kinetics by individual calculations of kinetic parameters for all possible ion number combinations which can occur in the system. Therefore, a reasonable description of the particle formation mechanism at molecular scale is guaranteed. This is of major importance because this mechanism is barely understood and no microemulsion-specific rate approaches are available up to now. Most investigations in this field are based on kinetic expressions being only valid for bulk phase processes. They neglect the discrete character of a small system, such as the ion-filled microemulsion droplets, where only countable amounts of ions exist in one droplet. They also do not consider the influence of the surfactant on particle nucleation and growth. Thus, the strong dependence of important parameters, like the critical amount of ions needed to form a stable nucleus, N_{crit}, from the ion distribution, was not being considered. Furthermore, no theoretical work addressed the question whether the large volume-specific surface area of the microemulsion droplets favours a heterogeneous nucleation mechanism or the question how the surfactant shells influence the particle growth rate, in particular when the particle size is limited by the droplet size.

2. Modeling

2.1. Model reduction

The here applied model reduction concept is based on some simplifying assumptions concerning the distributed properties of the system in order to obtain an efficient and reliable computational solution (for details see Öncül et al. [23]). According to these simplifications, the original population balance of droplets in terms of the three-dimensional number distribution $f_{ref}(N_A, N_B, N_P, t)$ is reduced to a set of two coupled population balances in terms of two number distribution functions of lower dimension. This is achieved by assuming that the reactant redistribution over the two daughter droplets during a fusion–fission event is independent of the existence and size of any particles within the droplets. The application of this assumption does not lead to a severe loss of generality because neither the influence of a particle on the redistribution behavior is proved at all nor a significant amount of exchange events of particle-filled droplets take place. This is due to the very low number of droplets containing a particle (<0.5%). The resulting distribution functions are a two-dimensional normalized density function $P_{2D}(N_A, N_B, t)$ and a one-dimensional droplet number distribution $f(N_P,t)$. With the just discussed assumption, the three-dimensional reference distribution f_{ref} can be expressed as product of two distributions of lower dimensions:

$$f_{ref}(N_A, N_B, N_P, t) = P_{2D}(N_A, N_B, t) \cdot f(N_P, t). \quad (3)$$

According to the separation approach in Eq. (3), the process model will consist of two coupled population balances, namely a droplet population balance in terms of P_{2D} which contains a droplet exchange term, and a droplet population balance in terms of f which contains nucleation and growth terms. Consequently, the integral term for the exchange mechanism appears in the two-dimensional population balance only, and this is why simulation results will be obtainable with a reasonable computational effort, i.e. in the order of a few hours.

But even this reduced model is still too complex with regard to the estimation of kinetic parameters for particle nucleation and growth rates. To further decrease the computational effort it is assumed that the distribution of ionic reactants over the droplet population is in equilibrium, i.e. the distribution function P_{2D} approaches an equilibrium distribution P_{2D}^{eq}. This hypothesis is motivated by the fact that the majority of droplets will not contain any particle and, consequently, the equilibrium droplet distribution is only slightly disturbed by exchange events of particle-containing droplets. It was shown by several authors (Atik and Thomas [42]; Hatton et al. [43]) that in particle-free systems different types of equilibrium distributions of ions will be established. The shape of these distributions depends on the interactions between the different ions. If cooperative and repulsive forces are almost equal, the ions will follow a Poisson distribution over the droplet population. If strong cooperative forces lead to the accumulation of ions in one droplet, the resulting distribution will have a bimodal shape. Thus, with the just discussed equilibrium hypothesis Eq. (3) simplifies to

$$f_{ref}(N_A, N_B, N_P, t) = P_{2D}^{eq}(N_A, N_B, t) \cdot f(N_P, t) \quad (4)$$

But in the real system droplet exchange events do not occur instantaneously, i.e. after depletion of those ionic species which are not in excess, new ions have to be transported into the droplet by successive exchange events. The time interval between two events slows down the particle formation rate. The equilibrium hypothesis ignores this slow-down effect, but the reduced model should still somehow reflect this important effect. The only model parameters, which can be used to account for this slow-down effect, are the kinetic constants occurring in the rate expressions for particle nucleation and growth. Thus, parameter estimation procedures which are based on the here discussed reduced model will always deliver “effective” kinetic parameters values which are masked by the influence of the droplet exchange phenomenon. But this model approach reduces the simulation time for one experiment down to the order of some seconds. Therefore, extensive parameter estima-

tion from experimental data can be performed, and the reduced model will be also suitable for applications in process control.

2.2. Population balance model

The population balance is formulated in terms of f which is the normalized droplet number distribution depending on N_P, the number of barium sulfate molecules in solid state. This balance is split into two subpopulation balances, namely one for particle-free droplets and one for droplets containing one single particle. The first subpopulation is described by an ODE with a sink term for nucleation and a source term for the external feed being added during semi-batch operation. The balance is given by:

$$\frac{\mathrm{d}f(0,t)}{\mathrm{d}t} = -\sum_{N_A=N_{crit}}^{N_{l,max}}\sum_{N_B=N_{crit}}^{N_{l,max}} P_{2D}^{eq}(N_A,N_B,t)\cdot r_{nuc}(N_A,N_B) \cdot\frac{V_{W,0}\cdot f(0,t)}{N_{M,0}} + \frac{N_{feed}(t)}{N_{M,0}}, \tag{5}$$

where $N_{l,max}$ is the maximum number of dissolved ions of one kind inside one droplet, r_{nuc} the nucleation rate, $V_{W,0}$ the total initial water volume in the reactor, N_{feed} the droplet feed rate and $N_{M,0}$ the initial total number of droplets inside the reactor. The double sum results from the fact that every possible droplet class, i.e. ion combination of N_A and N_B, has its individual growth rate because different supersaturation levels are established in each droplet class. By normalization with $N_{M,0}$ the time integral of f at the beginning ($t=0$) is 1 and after the feeding period ($t=t_{feed}$) is 2 if an equal volumes are mixed.

The second subpopulation balance is described by an ODE system with source terms for nucleation (only considered for classes where $N_{crit} \le N_P \le N_{l,max}$) and a discrete particle growth term:

$$\begin{aligned}\frac{\mathrm{d}f(N_P,t)}{\mathrm{d}t} = {} & \left[\sum_{i=0}^{N_{l,max}-N_P} P_{2D}^{eq}(N_P+i,N_P,t)\cdot r_{nuc}(N_P+i,N_P) + \sum_{i=1}^{N_{l,max}-N_P} P_{2D}^{eq}(N_P,N_P+i,t)\cdot r_{nuc}(N_P,N_P+i)\right] \cdot\frac{V_{W,0}\cdot f(0,t)}{N_{M,0}} + \sum_{N_A=1}^{N_{l,max}}\sum_{N_B=1}^{N_{l,max}} P_{2D}^{eq}(N_A,N_B,t) \\ & \cdot\left[\frac{f(N_P-1,t)}{\Delta d_{P,N_P-1}} r_{gro}(N_A,N_B,N_P-1) - \frac{f(N_P,t)}{\Delta d_{P,N_P}} r_{gro}(N_A,N_B,N_P)\right]\end{aligned} \tag{6}$$

where r_{gro} is the size-dependent particle growth rate and the Δd_P-values represent the particle size interval length for an equivalent sphere diameter difference. The relation between the internal coordinate N_P and the equivalent sphere diameter d_P is given by

$$d_P^3 = \frac{M_P}{k_V\cdot\rho_P\cdot N_{A^*}}\cdot N_P \tag{7}$$

where M_P is the mass of one $BaSO_4$ molecule, k_V is the volume shape factor ($\pi/6$ for a sphere), ρ_P the density of $BaSO_4$ and N_{A^*} Avogadro's number. As the nucleation term, the growth term in Eq. (6) is class-dependent, too. Thus, individual growth kinetics are accounted for in each droplet class (for $N_{A,max}=N_{B,max}=30$, this results in 900 different growth terms). Particle coagulation is not taken into account for the sake of short computation times. Moreover, coagulation only occurred in three of the ten here evaluated experiments which were presented in [1] and [2]. Thus, in the majority of the regarded experiments particle coagulation was not a dominant phenomenon.

2.3. Nucleation kinetics

For a reliable consideration of the nucleation mechanism in a small system ("small" with respect to the number of reactants within one droplet) it is very important to have a good approximation of the critical number of molecules forming a nucleus, N_{crit}. In literature, typical values for microemulsion processes are ranging between $N_{crit}=2$ (Jain and Mehra [30]) and $N_{crit}=8$ (Kumar et al. [31]), but for bulk precipitation values $N_{crit}>10$ are given (Kashchiev and van Rosmalen [44]). To the best of our knowledge, so far N_{crit} was never derived from the Gibbs–Thomson relation for microemulsion-assisted precipitation. In most works, N_{crit} was chosen as a fixed parameter for each droplet class with no relation to thermodynamic parameters of the system. Therefore, here we apply another approach, namely the following droplet-class-specific Gibbs–Thomson relation:

$$N_{crit}(S(N_A,N_B),\sigma_{eff}) = \frac{32\cdot\pi\cdot M_P^2}{\rho_P^2\cdot N_{A^*}^2}\cdot\frac{\sigma_{eff}^3}{3}\cdot(k_B\cdot T\cdot\ln(S(N_A,N_B)))^{-3} \tag{8}$$

where S is the supersaturation, σ_{eff} the effective interfacial surface tension, k_B the Boltzmann constant and T the temperature. According to Eq. (8), N_{crit} is not a constant parameter because it strongly depends on the supersaturation being established in each droplet class. The supersaturation in a droplet class can be calculated from the ion numbers N_A and N_B, the solubility K_L and the droplet volume V_D which is a constant parameter for microemulsions:

$$S(N_A,N_B) = \sqrt{\frac{c_A\cdot c_B}{K_L}} = \sqrt{\frac{N_A\cdot N_B}{K_L\cdot N_{A^*}^2\cdot V_D^2}}. \tag{9}$$

The effective interfacial surface tension σ_{eff} is the only uncertain parameter in Eq. (8). Its value depends on the underlying nucleation mechanism (homogeneous or heterogeneous). If the mechanism is known it is possible to estimate σ_{eff} as follows:

$$\sigma_{eff} = \sigma \quad \text{for homogeneous nucleation} \tag{10}$$

$$\sigma_{eff} = \xi^{1/3}(\Theta)\cdot\sigma \quad \text{for heterogeneous nucleation} \tag{11}$$

with $\xi(\Theta)=1/4(2+\cos\Theta)(1-\cos\Theta)^2$, where Θ is the wetting angle (see Kashchiev and van Rosmalen [44]). Values for the interfacial surface tension σ can be found in literature. These values vary between $\sigma=0.038$ and $0.187\,J/m^2$ (see Gilmer and Bennema [45], Dirksen and Ring [46], Nielsen and Söhnel [47] and Kashchiev and van Rosmalen [44]). Using these σ-values in Eq. (8), results in critical number in the range of $N_{crit}=1$–20 for homogeneous nucleation. This corresponds to the order of droplet occupancy of ions in our system. The latest and most reliable value is $\sigma=0.187\,J/m^2$, published by Kashchiev and van Rosmalen [44], which results in $N_{crit}=20$ for homogenous nucleation. Nevertheless, due to the uncertainty of this parameter (and thus the uncertainty of the underlying nucleation mechanism), we will estimate this parameter from own experimental data which were published previously in [1] and [2].

With the knowledge of N_{crit}, all supercritical droplet classes, i.e. classes with ion number combinations leading to the formation of a stable nucleus, can be determined. The nucleation rates in these classes are

$$r_{nuc}(N_A,N_B) = k_{nuc}^{eff}\cdot(S(N_A,N_B)-1)^{\alpha_{nuc}} \tag{12}$$

where k_{nuc}^{eff} stands for the effective nucleation rate constant and α_{nuc} for the effective nucleation rate order. Eq. (12) is adopted from bulk

phase kinetic approaches, see e.g. Baldyga et al. [48]. The supersaturation dependence in microemulsion is assumed to be similar to the corresponding bulk phase process. Here $\alpha_{nuc} = 15$ is used, as given in the work of Baldyga et al. [48]), due to the very high supersaturation inside the droplets ($S > 1000$ for one $BaSO_4$ molecule inside one droplet). The remaining unknown parameter, besides the effective interfacial surface tension σ_{eff}, is the nucleation rate constant k_{nuc}^{eff}. Both parameters were estimated from experimental data.

2.4. Growth kinetics

As stated above different mechanisms can be responsible for the observed growth behavior in the investigated system. In the present work four different approaches are compared in order to identify the most likely growth mechanism. The first approach (A) is used as reference kinetics. It corresponds to the standard bulk phase kinetic approach described by a power law expression in terms of the supersaturation S (see e.g. Nielsen [49]). The second approach (B) is a simplified crystal face-specific growth rate expression, the third approach (C) is an adsorption-related growth rate expression and the fourth approach (D) is a combination of B and C, which considers both, crystal face-specific growth velocities and surfactant adsorption effects.

2.4.1. Modified bulk phase approach

The standard bulk phase growth kinetics has a similar structure like the above described nucleation expression. In full analogy, the growth rate r_{gro} is calculated individually for each droplet class by using a droplet-specific supersaturation $S(N_A, N_B)$:

$$r_{gro}(N_A, N_B, N_P) = k_{gro}^{eff} \cdot (S(N_A, N_B) - 1)^{\alpha_{gro}} \quad (13)$$

where k_{gro}^{eff} stands for the effective growth rate constant and α_{gro} represents the effective growth rate order. As for nucleation kinetics, the dependence of supersaturation is assumed to be similar to the bulk phase process. The surface integration step is assumed to be rate limiting for particle growth which is based on the reasonable assumption that the diffusion resistance within the droplets is negligible. This corresponds to $\alpha_{gro} = 2$ (see Nielsen [49]. The effective growth rate constant k_{gro}^{eff} is used as a fitting parameter.

2.4.2. Crystal face-specific growth rates

The second approach accounts for crystal face-specific growth rates. The experimentally observed particles have a plate-like shape with a change during growth from a round main face to a rectangular and hexagonal main face (see Niemann et al. [1]). It is shown in Appendix A.1 how a crystal can be approximated as cuboid with plate-like shape and a dominant rectangular crystal face. The symmetry of this shape enables the application of a simplified face-specific growth rate approach for the three spatial directions x, y and z. A more general approach which considers arbitrary crystal shapes can be found, e.g. in Zhang and Doherty [26]. The derivation of the here applied simplified growth rate expression is given in Appendix A.2. Its final form sounds:

$$r_{gro}(N_A, N_B, N_P) = \frac{2}{\pi} \cdot \left[\frac{x(N_P) \cdot y(N_P)}{d_P(N_P)^2} \cdot G_z(N_A, N_B, N_P) + \frac{x(N_P) \cdot z(N_P)}{d_P(N_P)^2} \cdot G_y(N_A, N_B, N_P) + \frac{y(N_P) \cdot z(N_P)}{d_P(N_P)^2} \cdot G_x(N_A, N_B, N_P) \right] \quad (14)$$

where G_x, G_y and G_z are the crystal face-specific growth rates. They are expressed as functions of the droplet-class-specific supersaturation:

$$G_i(N_A, N_B, N_P) = k_{gro,i} \cdot (S(N_A, N_B) - 1)^{\alpha_{gro}} \quad (15)$$

where the individual growth rate constants $k_{gro,i}$ ($i = x, y, z$) are related to the overall growth rate constant k_{gro}^{eff} (see Appendix A.2). The particle diameter d_P is calculated from Eq. (7). The relation between the three particle dimensions (x, y, z) and the particle size N_P can be extracted from our experimental data (see Appendix A.1). Thus, this growth approach only contains one unknown parameter, k_{gro}^{eff}, which is to be estimated from experimental data.

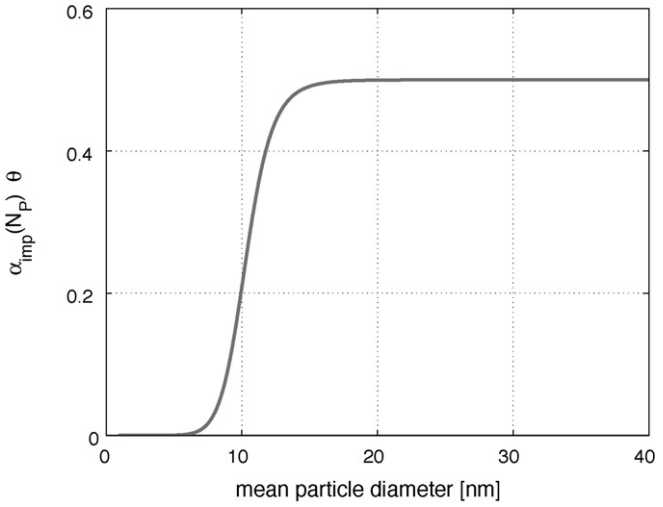

Fig. 2. Assumed function for the growth-rate reduction term (Eq. (17) with $a_1 = 0.5$, $a_2 = 4 \times 10^{-11}$ m^{-1}, $a_3 = 10$).

2.4.3. Surfactant adsorption-related growth rate

In our microemulsion precipitation experiments of barium sulfate, we found bulk-like growth for particles diameters below 6 nm, but for larger particles we found a significantly reduced growth rate [1] which may result from the direct adsorption of surfactant molecules on the nanoparticle surface. This motivates the formulation of a rate expression which accounts for the growth reduction by surfactant adsorption on the particle surface. Kubota and Mullin [25] considered this effect by introduction of the reduction term $\alpha_{imp} \cdot \theta$ (α_{imp}: factor for growth-rate reduction by impurities, here: surfactant molecules; θ: particle surface coverage of surfactant molecules). Using their approach, one can write down the following rate expression:

$$\begin{aligned} r_{gro}(N_A, N_B, N_P) &= (1 - \alpha_{imp}(N_P) \cdot \theta) \cdot r_{gro,0} \\ &= (1 - \alpha_{imp}(N_P) \cdot \theta) \cdot k_{gro}^{eff} \cdot (S(N_A, N_B) - 1)^{\alpha_{gro}} \end{aligned} \quad (16)$$

where $r_{gro,0}$ stands for the growth rate of particles in the surfactant-free system. In Eq. (16), both the term $\alpha_{imp}(N_P) \cdot \theta$ and the effective growth rate constant k_{gro}^{eff} are unknowns. The latter one can be estimated from experimental data. But for the term $\alpha_{imp}(N_P) \cdot \theta$ a reasonable function has to be assumed, because no rigorous expression is available in literature for the surfactant adsorption in this particular case. The following function is proposed here to describe the experimental findings:

$$\alpha_{imp}(N_P) \cdot \theta = a_1 \cdot \left(\frac{a_2 \cdot d_P(N_P)^{a_3}}{1 + a_2 \cdot d_P(N_P)^{a_3}} \right), \quad (17)$$

where a_1, a_2 and a_3 are unknown parameters to be identified from experimental data. Fig. 2 illustrates the shape of the function in Eq. (17).

2.4.4. Surfactant adsorption and face-specific growth rates

If both phenomena are influencing the particle growth behavior in microemulsions, i.e. different growth rates of crystal faces and surfactant adsorption on the particle surface, a combination of growth kinetics (B) and (C) should be applied. Then, the individual growth rates G_i in Eq. (14) are to be calculated as follows:

$$G_i(N_A, N_B, N_P) = (1 - \alpha_{imp}(N_P) \cdot \theta) \cdot k_{gro,i} \cdot (S(N_A, N_B) - 1)^{\alpha_{gro}}, \quad (18)$$

where the individual growth rate constants $k_{gro,i}$ are related to the overall growth rate constant k_{gro}^{eff} and the growth-rate reduction function is given by Eq. (17). Thus, this rate expression contains four parameters which have to be estimated, namely k_{gro}^{eff}, a_1, a_2 and a_3.

All four growth rate kinetics discussed above depend on the supersaturation level S which depends on the water volume inside a droplet V_D. This volume is assumed to be constant, i.e. independent of the size of the particle in the droplet. Due to particle growth, droplets are continuously expanded whereby more and more water molecules loose the state of free bulk water. In this transition situation, both the proportion of free water molecules within the considered droplet as well as water molecules of the second droplet participating in a fusion–fission event, influence the supersaturation level. Thus, the variation of the supersaturation by particle growth can be expected as being of minor importance. Once the particle size is close to the droplet size, the volume of free water is not changing any more because all water molecules of the droplet are bound to the surfactant molecules or the particle surface. In this situation, the supersaturation level is defined by the fusing droplets' water content which can be regarded as constant due to the microemulsion properties.

2.5. Equilibrium ion distribution P_{2D}^{eq}

The equilibrium distribution of dissolved ions in the droplet population at any time t is approximated by the two-dimensional Poisson probability density function in terms of the ion numbers of the reactants A and B, i.e. P_{2D}^{eq}. The use of this Poisson distribution is motivated by the work of Atik and Thomas [42] who showed analytically that this distribution will be established if cooperative and repulsive forces between the ions counterbalance each other exactly. But, it is important to note that the here proposed model formulation is also applicable to any other two-dimensional probability function. Thus, if more detailed information on the forces between ions becomes available in the future, the model can still be applied to other distribution, which will be non-Poissonian functions.

The Poisson distribution is given by

$$P_{2D}^{eq}(N_A, N_B, t) = P_A(N_A, t) \cdot P_B(N_B, t) \quad (19)$$

where the two individual Poisson distributions are calculated from

$$P_x(N_X, t) = \frac{\lambda_x(t)^{N_x}}{N_x!} \cdot e^{-\lambda_x(t)}; \quad x = A, B. \quad (20)$$

Thus, the two-dimensional Poisson distribution only contains two unknown parameters, namely the mean occupancies of the dissolved reactants A and B in the droplets, λ_A and λ_B respectively. At any time t, these occupancies can be calculated from the following equations:

$$\lambda_A(t) = \frac{N_A^t(t)}{N_M(t)}, \quad (21)$$

$$\lambda_B(t) = \frac{N_B^t(t)}{N_M(t)}, \quad (22)$$

where N_A^t and N_B^t are the total numbers of species A and B. N_M represents the total number of droplets inside the reactor. If A is fed to the semi-batch reactor, the latter three quantities can be easily determined from the following balance relations:

$$N_A^t(t) = (N_M(t) - N_{M,0}) \cdot \lambda_A^{feed}(t) - N_P^t(t), \quad (23)$$

$$N_B^t(t) = N_{M,0} \cdot \lambda_B(t = 0) - N_P^t(t), \quad (24)$$

$$\frac{dN_M(t)}{dt} = N_{feed}(t), \quad (25)$$

where N_P^t is the total number of A–B molecules in the whole population of particles and λ_A^{feed} is the mean occupancy of the droplets in the feed. N_P^t can be obtained from the particle distribution function $f(N_p,t)$.

3. Results and discussion

For the analysis of the particle formation mechanism with the here developed model, the unknown parameters of nucleation and growth kinetics were identified from own experimental data. Parameter estimation was achieved by simultaneous least squares fitting of ten experimentally obtained steady-state PSDs (see Niemann et al. [1] and Aditywarman et al. [2]) using the standard Simplex optimization algorithm implemented in Matlab7.1 (relative and absolute tolerance of 10^{-7}). Furthermore, a model sensitivity study w.r.t. the effective interfacial surface tension was

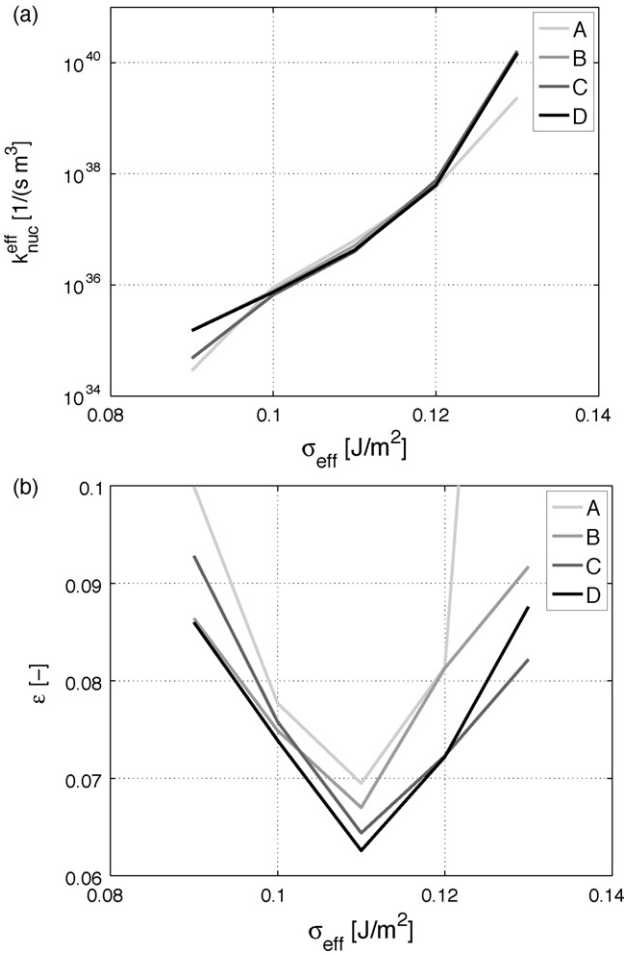

Fig. 3. (a) Influence of σ_{eff} and growth kinetics (A–D) on estimated nucleation constants (top); (b) Influence of σ_{eff} and growth kinetics (A–D) on the sum of errors between model data and experimental data (bottom).

performed in the parameter range from $\sigma_{eff} = 0.09$ to $0.13\,J/m^2$. According to Eq. (8), these surface tension values correspond to critical numbers from $N_{crit} = 3$ to 8.

Important conclusions for the analysis of the particle formation mechanism can be drawn from the two graphs which are shown in Fig. 3. The graph on the top shows the influence of the different growth mechanisms (A–D) and the effective surface tension (σ_{eff}) on the estimated nucleation rate constant, k_{nuc}^{eff}. The graph on the bottom shows the sum of errors versus the effective surface tension.

It can be seen in Fig. 3a that the estimated nucleation rate constant is almost independent of the applied growth rate approach, because the nucleation rate constant is linked to the number of created particles in the system, while it is not sensitive to the assumed growth mechanism. As can be seen from Fig. 3b, at a surface tension value of $\sigma_{eff} = 0.11\,J/m^2$ one gets the smallest error ε between experiments and simulations. From the Gibbs–Thomson relation, Eq. (8), the critical number of molecules forming a nucleus can be calculated: $N_{crit} = 5$–6. A comparison with the most recently published value for the interfacial surface tension $\sigma = 0.187\,J/m^2$ by Kashchiev and van Rosmalen [44] suggests heterogeneous nucleation as most probable mechanism for nuclei in the microemulsion system. Additionally, from Eq. (11) a reasonable value for the wetting angle, $\Theta \approx 65^\circ$, is obtained.

From Fig. 3b one sees that the growth rate approach (D) fits the experimental data best. This suggests that both effects, crystal face-specific growth velocities and surfactant adsorption, have an impact on particle growth. The most important factor in this combined kinetic approach seems to be surfactant adsorption and the – as a consequence – the existence of a growth barrier in case that the solid particle gets in contact to the droplet surface. When the two effects (three-dimensional growth and surfactant adsorption) are regarded separately (growth rate approaches B and C) the biggest

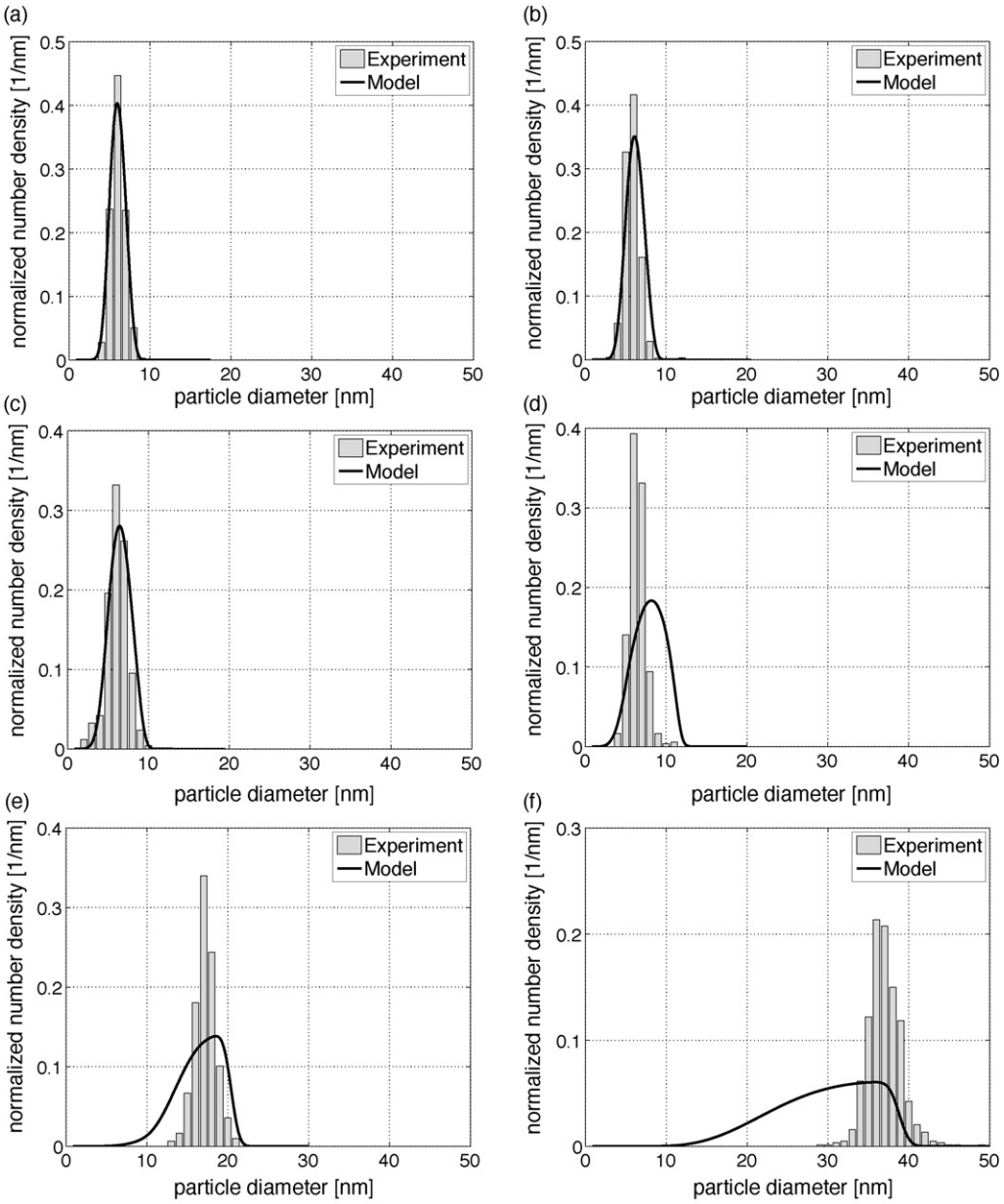

Fig. 4. Simulated versus experimental particle size distributions (PSD) at constant initial concentration in the reactor of $c_B = 0.1$ mol/l for six different initial concentrations in feed c_A. (a) PSD for $c_A = 0.1$ mol/l (top, left); (b) PSD for $c_A = 0.075$ mol/l (top, right); (c) PSD for $c_A = 0.05$ mol/l (middle, left); (d) PSD for $c_A = 0.025$ mol/l (middle, right); (e) PSD for $c_A = 0.01$ mol/(bottom, left); (f) PSD for $c_A = 0.005$ mol/l (bottom, right).

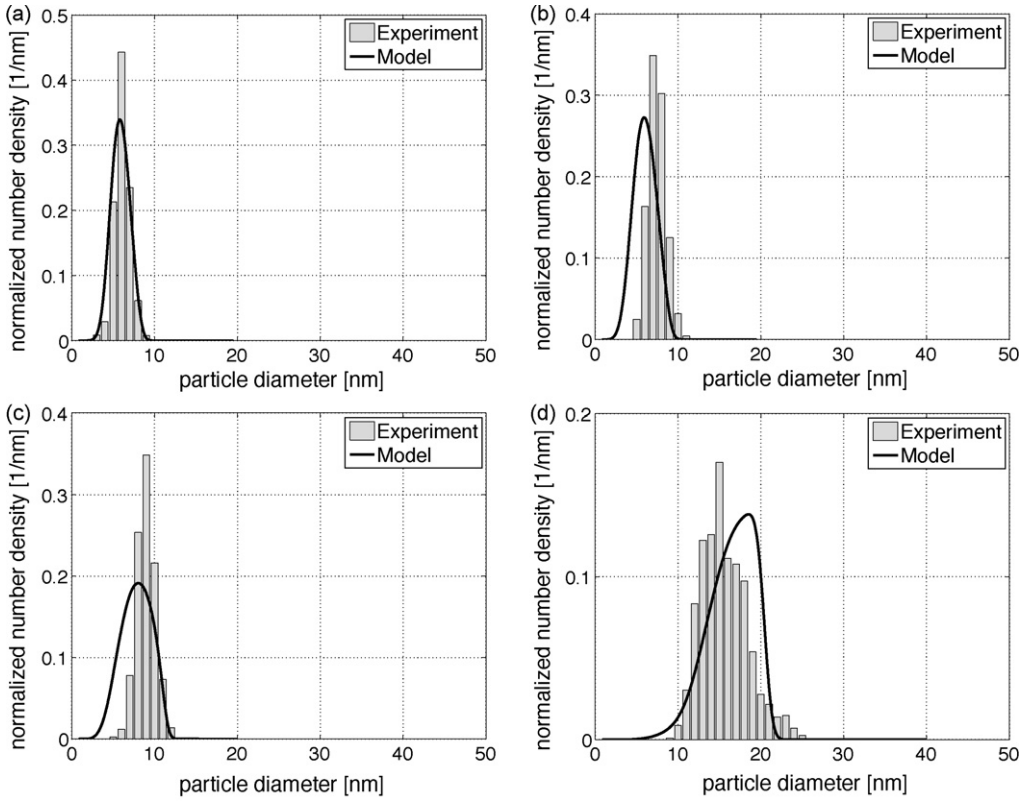

Fig. 5. Simulated versus experimental particle size distributions (PSD) at constant initial concentration in feed $c_A = 0.1$ mol/l for four different initial concentrations in the reactor c_B. (a) PSD for $c_B = 0.075$ mol/l (top, left); (b) PSD for $c_B = 0.05$ mol/l (top, right); (c) PSD for $c_B = 0.025$ mol/l (botton, left); (d) PSD for $c_B = 0.001$ mol/l (bottom, right).

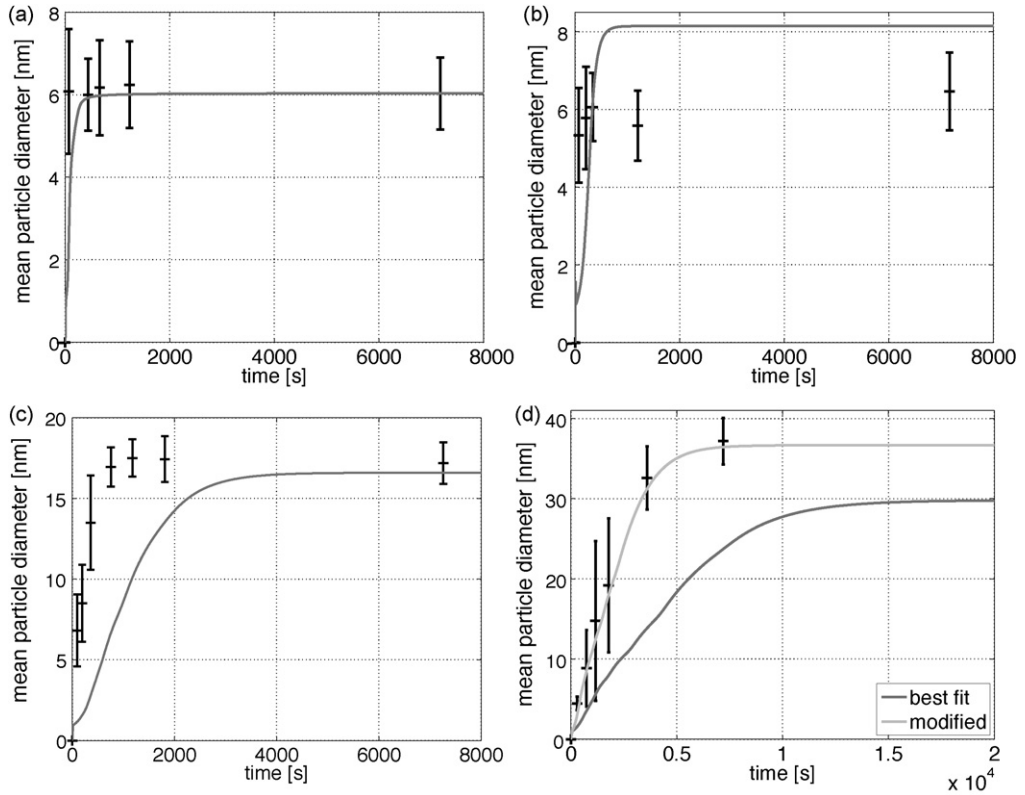

Fig. 6. Simulated versus experimental time evolution of mean particle diameter at constant initial concentration in the reactor of $c_B = 0.1$ mol/l for six different initial concentrations in feed c_A. (a) PSD for $c_A = 0.1$ mol/l (top, left); (b) PSD for $c_A = 0.025$ mol/l (middle, right); (c) PSD for $c_A = 0.01$ mol/(bottom, left); (d) PSD for $c_A = 0.005$ mol/l (bottom, right).

improvement compared to simple bulk kinetics (A) is obtained by approach (C), while (B) only results in a small improvement compared to (A). Please note that parameters a_2 and a_3 in Eq. (17) were not fitted, but were fixed.

In Fig. 4 the best fit of the experimental data is shown for six PSDs where the initial concentration in feed, c_A, was reduced step-wise from 0.1 to 0.005 mol/l while the initial concentration inside reactor droplets, c_B, was kept constant at 0.1 mol/l (for details see Niemann et al. [1]). The quality of the fit for the PSDs where the concentration in the reactor was reduced stepwise is comparable (see Fig. 5). The simulations were performed with $\sigma_{eff} = 0.11\,J/m^2$ using growth kinetics according to approach (D). The optimized parameters are $k_{nuc}^{eff} = 1.03 \times 10^{38}\,s^{-1}\,m^3$, $k_{gro}^{eff} = 74\,nm\,s^{-1}$, $a_1 = 0.39$, $a_2 = 4 \times 10^{-11}\,m^{-1}$ and $a_3 = 10$ ($\varepsilon = 0.0648$). A qualitatively good agreement with the experiments is achieved, as can be seen in Fig. 4a–c and e ($\Delta c_0 = 0$, 0.025, 0.05 and 0.09 mol/l, see Eq. (2)). In all these cases the location, shape and broadness of the PSDs are almost similar. The small deviation in Fig. 4d ($\Delta c_0 = 0.075$ mol/l) can be explained by the adjacency to the growth barrier. If the PSDs for this state from Adityawarman et al. [2] and Niemann et al. [1] are compared, it can be seen that the particles obtained by Adityawarman et al. [2] are larger. It can be concluded that small interferences close to the barrier can lead to significantly different results. The fit for the last experiment with the maximum initial concentration difference $\Delta c_0 = 0.095$ mol/l (see Fig. 4f) shows significant differences of simulated and experimental PSDs. In that case, the mean particle size is too small and the simulated PSD is too broad compared to the experimental results. This deviation might result from the neglect of particle coagulation in the here applied model.

In addition to steady-state results, we analyzed the dynamic evolution of the mean particle diameter over time during four semi-batch experiments. As can be seen from Fig. 6), generally experimental and simulated dynamics are in reasonable qualitative agreement. Please note that the simulated process dynamics were obtained with parameters being fitted to steady-state data only. The agreement in Fig. 6a is very good, while the response time in Fig. 6c is too slow. Nevertheless, the predicted mean particle diameter is correct in this case. Correctly predicted dynamics can be also seen in Fig. 6b for conditions close to the growth barrier. Here only the mean particle diameter is slightly over-predicted due to the reasons explained above. For the most extreme initial concentration difference $\Delta c_0 = 0.095$ mol/l (see Fig. 6d), simulated dynamics are much slower than experimentally observed dynamics (best fit curve). If the growth rate constant is multiplied by a factor of three, the response curve represented by the gray line (modified) is obtained which fits the experimental observations quantitatively very good. The applied growth rate approach without consideration of particle coagulation might be the reason for these deviations at high Δc_0-values. To clarify this aspect, a detailed analysis of the particle formation mechanism at finite droplet exchange kinetics should be performed in the future, using a rigorous process model which relaxes the assumptions being made in the here presented reduced model.

4. Conclusions

The presented discrete population balance model in combination with the applied separation approach and the equilibrium hypothesis for the distribution of the dissolved reactants leads to an efficient numerical scheme for the simulation of the precipitation of *BaSO4* nanoparticles inside the droplets of a microemulsion. The low computational effort and the high accuracy of the obtained solution are major prerequisites for the applicability of this model for parameter estimation, process analysis and process control. Therefore, it was possible to analyze the particle formation mechanism in reverse microemulsion under extensive variation of model parameters. Comparison of identified parameter values with literature data [44] leads to the conclusion that nuclei are formed heterogeneously with a typical critical nucleus size of $N_{crit} = 5$–6, depending on the considered droplet class. The particle growth mechanism seems to be significantly influenced by three-dimensional face-specific growth effects and by the adsorption of surfactants.

The analysis of dynamic data leads to the conclusion that the micro-kinetics of particle formation in microemulsion droplets, in particular at the growth barrier, deserves a more detailed investigation. The coagulation of particles is also not well understood. Furthermore, cooperative and repulsive forces between ions might play a role for their redistribution behavior in the microemulsion droplets. To include these forces in an appropriate way, droplet exchange dynamics have to be modeled by an additional two-dimensional population balance in terms of discrete ion numbers whereby substituting the equilibrium hypothesis. This is subject of our current research activities.

Appendix A

A.1. Experimental analysis of the particle shape

Niemann et al. [1] presented an analysis of the crystal shape dynamics of the investigated system. They showed that particles with a size below the growth barrier have an almost round shape while particles which crossed the barrier change their shape during growth. Particles close to the barrier have a plate-like shape with a dominant rectangular face and larger particles have a plate-like shape with a hexagonal main crystal face. A complete three-dimensional characterization of the round particles from the TEM was not possible due to their small size; therefore at first the larger particles were analyzed. The analysis shown in the following is not completely given in our experimental work (Niemann et al. [1]), because the dependencies of x, y and z are only needed in the theoretical analysis of the growth rate approach.

The dominant rectangular and hexagonal crystal faces have the same x/y ratio if the hexagonal face is transformed in a rectangular face like shown in Fig. A1. The ratio is determined by the individual measurement of these length scales from all particles observed on the TEM pictures. With an angle α_{hex} of 36° (mean value, measured values are between 33° and 45°) the ratio is given by

$$\frac{x}{y} = 1.5 - \frac{1}{2} \cdot \tan(\alpha_{hex}). \tag{A1}$$

The dependence of the particle thickness z from x is obtained by an exponential function fit (trend-line) of the experimental data to

$$z = 0.74 \cdot x^{0.83}\,[nm]. \tag{A2}$$

With the knowledge of these dependencies it is possible to define the three-dimensional particle shape by one equivalent sphere diameter from the condition that the volumes have to be equal. The dependence of x from the mean particle diameter d_P (and therefore as well N_P according to Eq. (7)) is then given by

$$V_P = x \cdot y \cdot z = x \cdot \frac{x}{1.5 - 0.5 \cdot \tan(\alpha_{hex})} \cdot 0.74 \cdot x^{0.83} = k_P^x \cdot x^{2.83} = \frac{\pi}{6} \cdot d_P^3. \tag{A3}$$

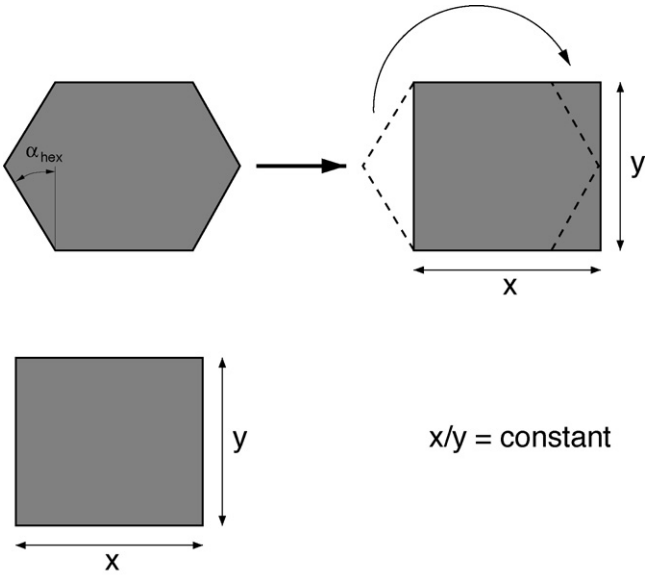

Fig. A1. Transformation of a hexagonal area into a rectangular area at constant x/y ratio.

Consequently, the dependencies of y and z can be derived from Eqs. (A1) and (A2). Fig. A2 shows all of these dependencies graphically. The graphs shown in this figure are validated for a particle size above 10 nm. Nevertheless, the extrapolated data for smaller particles match the experimental data qualitatively good. The volumes calculated from x, y and z are comparable with the equivalent sphere volumes from the measured d_P-values and therefore these correlations are used for all particle sizes in our model equations.

A.2. Derivation of Eq. (14) and calculation of $k_{gro,i}$

The general definition of the growth rate is given by

$$r_{gro} = \frac{dd_P}{dt}. \tag{A4}$$

The volume of a spherical crystal is calculated by

$$V_P = \frac{\pi}{6} d_P^3. \tag{A5}$$

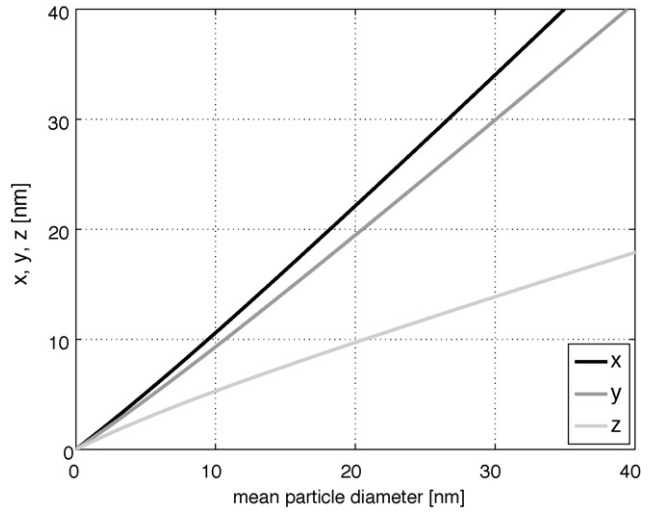

Fig. A2. Experimentally determined correlation between x, y and z and the mean particle diameter (equivalent sphere).

Inserting Eq. (A5) in Eq. (A4) results in

$$\frac{d}{dt} V_P = \frac{\pi}{6} \frac{d}{dt} d_P^3 = \frac{\pi}{6} 3 d_P^2 \frac{dd_P}{dt} = \frac{\pi}{2} d_P^2 \cdot r_{gro}. \tag{A6}$$

The volume of a cuboid is calculated by

$$V_P = x \cdot y \cdot z. \tag{A7}$$

The time derivative of Eq. (A7) is

$$\frac{d}{dt} V_P = x \cdot y \cdot \frac{dz}{dt} + x \cdot z \cdot \frac{dy}{dt} + y \cdot z \cdot \frac{dx}{dt} \tag{A8}$$

and if the cuboid has the same volume like the spherical particle Eq. (A6) has to be equal to Eq. (A8) which results in the following growth rate definition

$$r_{gro} = \frac{2}{\pi} \cdot \left[\frac{x \cdot y}{d_P^2} \cdot \frac{dz}{dt} + \frac{x \cdot z}{d_P^2} \cdot \frac{dy}{dt} + \frac{y \cdot z}{d_P^2} \cdot \frac{dx}{dt} \right] \tag{A9}$$

with $dx/dt = G_x$, $dy/dt = G_y$ and $dz/dt = G_z$.

If a similar growth rate approach is used for G_x, G_y and G_z (see Eq. (15)) and the particle shape evolution is a known function (see Appendix A.1) the following correlation between the individual growth constants has to be taken into account

$$\frac{dx}{dy} = \frac{G_x}{G_y} = \frac{k_{gro,x}}{k_{gro,y}} \tag{A10}$$

and

$$\frac{dx}{dz} = \frac{G_x}{G_z} = \frac{k_{gro,x}}{k_{gro,z}}. \tag{A11}$$

This means that all individual growth rate constants can be related to one of these growth rate constants ($k_{gro,x} = k_{gro}^{eff}$) by geometric considerations and thus only one of these constants has to be optimized by the parameter estimation procedure.

References

[1] B. Niemann, P. Veit, K. Sundmacher, Nanoparticle precipitation in reverse microemulsions: particle formation dynamics and tailoring of particle size distributions, Langmuir 24 (1) (2008) 4320–4328.
[2] D. Adityawarman, A. Voigt, P. Veit, K. Sundmacher, Precipitation of $BaSO_4$ nanoparticles in a non-ionic microemulsion: identification of suitable control parameters, Chem. Eng. Sci. 60 (12) (2005) 3373–3381.
[3] K.J. Klabunde, Nanoscale Materials in Chemistry, John Wiley & Sons, Inc., New York, 2001, p. 292.
[4] W. Luther, Industrial application of nanomaterials—chances and risks. Technological analysis, in: W. Luther (Ed.), Future Technologies, vol. 54, Future Technologies Division of VDI Technologiezentrum GmbH, Düsseldorf, 2004, p. 119.
[5] C.N.R. Rao, A. Müller, A.K. Cheetham, The Chemistry of Nanomaterials. Synthesis, Properties and Applications in 2 Volumes, vol. 1, WILEY-VCH Verlag GmbH & Co KgaA, Weinheim, 2004.
[6] M. Boutonnet, J. Kizling, P. Stenius, The preparation of monodisperse colloidal metal particles from microemulsions, Colloids Surf. 5 (3) (1982) 209–225.
[7] H. Sato, T. Ohtsu, I. Komasawa, Preparation of ultrafine palladium particles in reverse micelles and application for hydrogenation catalysts, J. Chem. Eng. Jpn. 35 (3) (2002) 255–262.
[8] M.L. Wu, D.H. Chen, T.C. Huang, Preparation of Pd/Pt bimetallic nanoparticles in water/AOT/isooctane microemulsions, J. Colloid Interface Sci. 243 (1) (2001) 102–108.
[9] G.L. Li, G.H. Wang, Synthesis of nanometer-sized TiO_2 particles by a microemulsion method, Nanostruct. Mater. 11 (5) (1999) 663–668.
[10] T. Hirai, H. Sato, I. Komasawa, Mechanism of formation of titanium-dioxide ultrafine particles in reverse micelles by hydrolysis of titanium tetrabutoxide, Ind. Eng. Chem. Res. 32 (12) (1993) 3014–3019.
[11] J.B. Nagy, Multinuclear NMR characterization of microemulsions—preparation of monodisperse colloidal metal boride particles 35 (2–4) (1989) 201–220.
[12] K. Kandori, K. Konno, A. Kitahara, Formation of ionic water oil microemulsions and their application in the preparation of $CaCO_3$ particles, J. Colloid Interface Sci. 122 (1) (1988) 78–82.
[13] P. Monnoyer, A. Fonseca, J.B. Nagy, Preparation of colloidal AgBr particles from microemulsions, Colloid Surf. A-Physicochem. Eng. Asp. 100 (1995) 233–243.

[14] F. Debuigne, J. Cuisenaire, L. Jeunieau, B. Masereel, J.B. Nagy, Synthesis of nimesulide nanoparticles in the microemulsion epikuron/isopropyl myristate/water/n-butanol (or isopropanol), J. Colloid Interface Sci. 243 (1) (2001) 90–101.
[15] T. Hirai, H. Sato, I. Komasawa, Mechanism of formation of CdS and ZnS ultrafine particles in reverse micelles, Ind. Eng. Chem. Res. 33 (12) (1994) 3262–3266.
[16] M.P. Pileni, L. Motte, F. Billoudet, C. Petit, Synthesized "in situ" in reverse micelles of silver-sulfide semiconductors, Surf. Rev. Lett. 3 (1) (1996) 1215–1218.
[17] L.M. Qi, J.M. Ma, H.M. Cheng, Z.G. Zhao, Preparation of $BaSO_4$ nanoparticles in non-ionic w/o microemulsions, Colloid Surf. A-Physicochem. Eng. Asp. 108 (1) (1996) 117–126.
[18] N.I. Ivanova, D.S. Rudelev, B.D. Summ, A.A. Chalykh, Synthesis of barium sulfate nanoparticles in water-in-oil microemulsion systems, Colloid J. 63 (6) (2001) 714–717.
[19] R. Bandyopadhyaya, R. Kumar, K.S. Gandhi, Modelling of $CaCO_3$ nanoparticle formation during overbasing of lubricating oil additives, Langmuir 17 (4) (2001) 1015–1029.
[20] R. Bandyopadhyaya, R. Kumar, K.S. Gandhi, Simulation of precipitation reactions in reverse micelles, Langmuir 16 (18) (2000) 7139–7149.
[21] P. Kumar, K.L. Mittal (Eds.), Handbook of Microemulsion Science and Technology, Marcel Dekker Inc., New York, 1999.
[22] F. Rauscher, P. Veit, K. Sundmacher, Analysis of a technical-grade w/o microemulsion and its application for the precipitation of calcium carbonate nanoparticles, Colloid Surf. A-Physicochem. Eng. Asp. 254 (1–3) (2005) 183–191.
[23] A. Öncül, B. Niemann, K. Sundmacher, D. Thévenin, CFD modelling of BaSO4 precipitation inside microemulsion droplets in a semi-batch reactor, Chem. Eng. J. 138 (2008) 498–509.
[24] S. Mann, G.A. Ozin, Synthesis of inorganic materials with complex form, Nature 382 (6589) (1996) 313–318.
[25] N. Kubota, J.W. Mullin, A kinetic model for crystal-growth from aqueous-solution in the presence of impurity, J. Cryst. Growth 152 (3) (1995) 203–208.
[26] Y.C. Zhang, M.F. Doherty, Simultaneous prediction of crystal shape and size for solution crystallization, AIChE J. 50 (9) (2004) 2101–2112.
[27] B. Niemann, K. Sundmacher, Nanoparticle precipitation in microemulsion: a discrete-continuous Population Balance approach, in: PARTEC 2007, Nürnberg, Germany, 2007.
[28] B. Niemann, F. Rauscher, D. Adityawarman, A. Voigt, K. Sundmacher, Microemulsion-assisted precipitation of particles: experimental and model-based process analysis, Chem. Eng. Process. 45 (10) (2006) 917–935.
[29] R. Bandyopadhyaya, Modelling of precipitation in reverse micelles, in: Chemical Engineering Department, Indian Institute of Science, Bangalore, India, 2000, p. 226.
[30] R. Jain, A. Mehra, Monte Carlo models for nanoparticle formation in two microemulsion systems, Langmuir 20 (15) (2004) 6507–6513.
[31] A.R. Kumar, G. Hota, A. Mehra, K.C. Khilar, Modeling of nanoparticles formation by mixing of two reactive microemulsions, AIChE J. 50 (7) (2004) 1556–1567.
[32] Y.C. Li, C.W. Park, Particle size distribution in the synthesis of nanoparticles using microemulsions, Langmuir 15 (4) (1999) 952–956.
[33] U. Natarajan, K. Handique, A. Mehra, J.R. Bellare, K.C. Khilar, Ultrafine metal particle formation in reverse micellar systems: effects of intermicellar exchange on the formation of particles, Langmuir 12 (11) (1996) 2670–2678.
[34] C. Tojo, M.C. Blanco, M.A. Lopez-Quintela, Microemulsions as microreactors: a Monte Carlo simulation on the synthesis of particles, J. Non-Cryst. Solids 235 (1998) 688–691.
[35] C. Tojo, M.C. Blanco, M.A. Lopez-Quintela, Preparation of nanoparticles in microemulsions: a Monte Carlo study of the influence of the synthesis variables, Langmuir 13 (17) (1997) 4527–4534.
[36] C. Tojo, M.C. Blanco, F. Rivadulla, M.A. Lopez-Quintela, Kinetics of the formation of particles in microemulsions, Langmuir 13 (7) (1997) 1970–1977.
[37] S. Quintillan, C. Tojo, M.C. Blanco, M.A. Lopez-Quintela, Effects of the intermicellar exchange on the size control of nanoparticles synthesized in microemulsions, Langmuir 17 (23) (2001) 7251–7254.
[38] R. Bandyopadhyaya, R. Kumar, K.S. Gandhi, D. Ramkrishna, Modeling of precipitation in reverse micellar systems, Langmuir 13 (14) (1997) 3610–3620.
[39] H. Sato, T. Hirai, I. Komasawa, Mechanism of formation of composite CdS-ZnS ultrafine particles in reverse micelles, Ind. Eng. Chem. Res. 34 (7) (1995) 2493–2498.
[40] H. Sato, T. Ohtsu, I. Komasawa, Improvement of the productivity of preparation process for ultrafine metal sulfide particles using reverse micellar systems, J. Chem. Eng. Jpn. 32 (3) (1999) 300–306.
[41] A. Voigt, B. Niemann, K. Sundmacher, Model-based process evaluation of nanoparticle precipitation in microemulsions, in: 13th International Workshop on Industrial Crystallization, BIWIC 2006, 13th–15th September, Delft, The Netherlands, 2006.
[42] S.S. Atik, J.K. Thomas, Transport of photoproduced ions in water in oil microemulsions—movement of ions from one water pool to another, J. Am. Chem. Soc. 103 (12) (1981) 3543–3550.
[43] T.A. Hatton, A.S. Bommarius, J.F. Holzwarth, Population-dynamics of small systems. 1. Instantaneous and irreversible reactions in reversed micelles, Langmuir 9 (5) (1993) 1241–1253.
[44] D. Kashchiev, G.M. van Rosmalen, Review: nucleation in solutions revisited, Cryst. Res. Technol. 38 (7–8) (2003) 555–574.
[45] G.H. Gilmer, P. Bennema, Simulation of crystal-growth with surface diffusion, J. Appl. Phys. 43 (4) (1972) 1347–1360.
[46] J.A. Dirksen, T.A. Ring, Fundamentals of crystallization: kinetic effects on particle size distributions and morphology, Chem. Eng. Sci. 46 (10) (1991) 2389–2427.
[47] A.E. Nielsen, O. Söhnel, Interfacial tensions electrolyte crystal-aqueous solution, from nucleation data, J. Cryst. Growth 11 (3) (1971) 233–242.
[48] J. Baldyga, W. Podgorska, R. Pohorecki, Mixing-precipitation model with application to double feed semibatch precipitation, Chem. Eng. Sci. 50 (8) (1995) 1281–1300.
[49] A.E. Nielsen, Electrolyte crystal-growth mechanisms, J. Cryst. Growth 67 (2) (1984) 289–310.